TU Delft

Delft University of Technology

Document Version
Final published version

Licence
Dutch Copyright Act (Article 25fa)

Citation (APA)
Li, S., Xie, L., Wang, M., Li, H., & Lu, C. (2026). Multi-parameter interaction optimization for dynamic energy matching in PV driven air conditioning with different BIPV types. *Energy and Buildings*, *357*, Article 117186. https://doi.org/10.1016/j.enbuild.2026.117186

Important note
To cite this publication, please use the final published version (if applicable).
Please check the document version above.

Copyright
In case the licence states “Dutch Copyright Act (Article 25fa)”, this publication was made available Green Open Access via the TU Delft Institutional Repository pursuant to Dutch Copyright Act (Article 25fa, the Taverne amendment). This provision does not affect copyright ownership.
Unless copyright is transferred by contract or statute, it remains with the copyright holder.

Sharing and reuse
Other than for strictly personal use, it is not permitted to download, forward or distribute the text or part of it, without the consent of the author(s) and/or copyright holder(s), unless the work is under an open content license such as Creative Commons.

Takedown policy
Please contact us and provide details if you believe this document breaches copyrights.
We will remove access to the work immediately and investigate your claim.

This work is downloaded from Delft University of Technology.

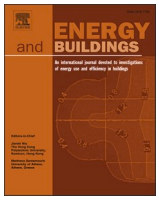
Energy & Buildings 357 (2026) 117186



Contents lists available at ScienceDirect

Energy & Buildings

journal homepage: www.elsevier.com/locate/enb





Multi-parameter interaction optimization for dynamic energy matching in PV driven air conditioning with different BIPV types

Sihui Li [a,b], Li Xie [a], Meng Wang [a,*], Houpei Li [b,c], Chujie Lu [d]

[a] College of Energy and Power Engineering, Changsha University of Science and Technology, Changsha 410114, PR China
[b] Key Laboratory of Building Safety and Energy Efficiency (Hunan University), Ministry of Education, PR China
[c] College of Civil Engineering, Hunan University, Changsha 410082, PR China
[d] Department of Architectural Engineering and Technology, Delft University of Technology, Juliana Laan 134, 2628 BL Delft, Netherlands (the)

ARTICLE INFO

Keywords:
Photovoltaic driven air conditioning
Building integrated photovoltaic
Zero energy building
Energy saving
Energy matching

ABSTRACT

PV driven air conditioning (PVAC) systems integrated with building integrated photovoltaics (BIPV) are critical for achieving nearly zero energy buildings (NZEBs). Building design parameters simultaneously affect both PV generation and building load demand, yet the complex interactions among these parameters and their collective impact on dynamic energy matching are not well understood. This oversight frequently leads to suboptimal system performance. This study proposes a dynamic energy matching evaluation and optimization framework for PVAC-BIPV systems, incorporating physical models of their energy interactions and employing a systematic, multi-parameter approach to optimize building design parameters in different climatic regions. The maximum relative error of the simulation model for buildings integrated with various BIPV types is 9.80%. Univariate analysis reveals a clear hierarchy of influence, identifying shape factor as the most dominant parameter, followed by window-to-wall ratio (WWR) and then orientation. More importantly, the interaction between shape factor and WWR was identified as the most critical synergistic pairing, governing both available PV area and cooling demand. Through individual adjustment, synergistic combinations, and full-parameter optimization, the system achieved maximum SS improvements of 33.58% in Guangzhou and 24.21% in Shanghai, yielding ultimate SS values of 76.26% and 83.84%, respectively. The final designs for each region are characterized by their optimal parameter sets (45°, 0.555, 0.2) in Shanghai and (60°, 0.555, 0.2) in Guangzhou. The framework has great significance for the climate-adaptive design of PVAC integrated with BIPV types to achieve nearly ZEBs targets.

1. Introduction

1.1. Background

Energy consumption of buildings accounts for approximately 33% of global energy consumption [1]. In this context, the concept of near zero energy buildings (ZEBs) has emerged as a pivotal strategy [2]. A zero energy building refers to a building that produces as much energy as it consumes in a defined period. The main fundamental steps to achieve ZEBs are reducing energy consumption in buildings and using renewable energy to cover energy consumption [3].

Renewable energy resources include many types, such as solar, wind, biofuel, geothermal, etc. Due to technological advances and the price of photovoltaic (PV) products, PV technology has grown sharply in recent decades. Building Integrated Photovoltaics (BIPV) types have been one of the most suitable PV technologies to balance energy consumption for achieving near ZEBs [4]. Among various BIPV technologies, there are many different installation locations of PV on buildings to increase PV generation, including roofs, facades, skylights, and shading systems [5]. Most PV applications limit the installation to the horizontal surface of the building, especially rooftops, to maximize PV production. However, urbanization has led to a significant increase in high-rise buildings, decreasing the proportion of rooftop area relative to the total building surface [6,7]. Furthermore, rooftop spaces are often constrained by HVAC equipment and elevator shafts. To bridge this energy gap, the integration of PV modules on the vertical façade has become increasingly popular [8,9], with a particular focus on south-facing installations [10,11]. To further improve PV generation, some researchers have investigated the BIPV system's energy performance combined with south, west, and east walls [12,13]. Unlike rooftop PV, BIPV façades

* Corresponding author.
E-mail address: wangmeng@csust.edu.cn (M. Wang).

https://doi.org/10.1016/j.enbuild.2026.117186
Received 6 November 2025; Received in revised form 28 December 2025; Accepted 17 February 2026
Available online 18 February 2026
0378-7788/© 2026 Elsevier B.V. All rights are reserved, including those for text and data mining, AI training, and similar technologies.

serve a dual function to achieve a higher energy matching degree. They generate electricity and simultaneously act as part of the building envelope, regulating solar heat gain and thermal insulation, which directly influences the building's cooling load [14,15].

PV direct-driven air conditioning (PVAC) systems can consume generation of PV facades to satisfy the indoor thermal comfort requirements, which is one of the most efficient technologies to achieve a near ZEBs target [16]. However, the integration of PVAC with BIPV establishes a highly complex energy system, inevitably leading to substantial real-time energy mismatches. This mismatch is further exacerbated by the complex coupling between building design parameters and system operation performance. Specifically, design parameters such as shape factor and Window-to-Wall Ratio (WWR) often exert conflicting dual influences on energy supply and demand for PVAC-BIPV systems simultaneously. Consequently, traditional static or isolated design approaches are insufficient to address this dynamic energy mismatching, necessitating a systematic framework that considers these multi-parameter interactions.

1.2. Related work on the energy performance of different BIPV types

In recent decades, the energy performance of different BIPV types has been extensively studied [17,18]. Wang et al. and Bhuvad et al. studied the energy-saving efficiency of PV rooftop systems considering the benefit of PV energy generation and shading [19,20]. With the recent development of PV integration on the vertical building surface, the energy performance of the BIPV system has been extensively studied [21,22]. Ji et al. simulated the thermal and electrical performance of a PV wall system under different operation conditions in Hong Kong [23]. Scharm et al. have accessed the impacts of PV facades on the load demand of buildings, which can reduce the load demand to some extent [24,25]. Gjorgievski et al. investigated the energy matching between the generation of PV roofs and energy consumption of air conditioning [25], and found the annual self-consumption of households is only 48.17% with 3 kWp PV generation.

To improve energy matching between PV generation and building load demand, several studies have been conducted on the energy performance of different PV facades. Laura et al. investigated the impact of PV roofs on the energy balance of building [26]. Feng et al. assessed the power generation potential and feasibility of achieving ZEBs with different BIPV types under different climate zones in China, and emphasized the contribution of PV façades [27]. To further explore the impact of climatic diversity on emerging BIPV technologies, Chung et al. established performance level criteria for semi-transparent PV windows, emphasizing that optimal optical and thermal properties are critical for achieving net-zero energy targets [46,47]. These work underscore that BIPV performance is sensitive to the local climatic conditions. Jeongyoon et al. estimated the building energy demand and the generation of PV façade in Korea [28]. Daniel et al. obtained the daily PV generation with the south PV façade and electricity consumed by building electrical equipment [29]. It is necessary to integrate the battery energy storage system to improve the energy matching degree. Due to the fluctuation of PV generation and AC energy consumption, the real-time energy mismatching problem of PVAC systems is serious, which will restrict the development of BIPV and PVAC technologies.

Since the PV facades with different orientations not only increase the total energy generation but also regulate the output power curve, the west and east PV facades have been investigated too. Liu et al. [30] conducted the energy matching between load demand and energy generation of PV façade and rooftop. The result shows that the PV generation can cover 79% of load demand in a low-rise building with a combination of roof, south, east, and west façade. This means that the PVAC system with different BIPV types has greater potential for reaching real-time energy matching. However, these studies seldom consider the interaction between BIPV types and building envelopes in the discussion, the energy matching degree may be not very accurate.

1.3. Related work on the optimization of different BIPV types

The incident solar radiation on the building surface is an essential variable in determining the energy generation of the BIPV system [31]. Some researchers have studied the application of PV rooftops with different tilt angles and azimuth angles in different climatic regions. Results indicated that a PV rooftop can cover over 50% of building load demand in low-rise buildings in tropical regions [32–34]. Except for PV rooftops, the optimization of PV façade also contributes to achieving near ZEBs. Vassiliades pointed out that the orientation of the BIPV modules (i.e., tilt angle and azimuth angle) can influence the received solar radiation [35,36]. Chatzipanagi et al. studied the electrical and thermal performance of BIPV types with different inclination angles [37]. When PV modules are installed on the exterior wall of the building, the tilt angle of the PV module is restricted for safety. This implies that most PV modules are conducted in a manner parallel to the wall. The energy performance optimization of PV façade is also affected by some important factors such as the building type, location, and climatic conditions [38,39]. The building shape factor, which constitutes the relationship between the exposed surface areas and the floor areas, significantly affects the energy generation of BIPV types [40,41]. Regarding the PV façade, the findings show that the window-to-wall ratio(WWR) also contributes to the PV installed capacity variation and the building load demand, which can be the preferred optimization variable to enhance the BIPV's energy performance [42,43].

In general, most existing optimization studies have relied on univariate approaches, treating the minimization of building load demand and the maximization of BIPV generation as decoupled objectives. This methodology fails to address the complex coupling effects inherent in PVAC-BIPV systems, where design parameters often exert conflicting dual influences on energy supply and demand. For instance, increasing the WWR simultaneously constrains the effective area for PV generation while intensifying solar heat gain. Similarly, a larger Shape Factor expands BIPV capacity but inevitably amplifies the envelope's thermal exposure. Given these inherent contradictions, isolated parameter optimization often yields suboptimal solutions that fail to balance the dynamic supply–demand equilibrium. Therefore, a systematic framework explicitly considering these multi-parameter interactions is essential.

1.4. Gap and proposed solution

While substantial literature exists on energy performance and design optimization of BIPV systems, a critical gap remains in addressing the dynamic energy matching between PV generation and AC consumption, particularly under the complex coupling of diverse BIPV typologies and building design. Building surfaces integrated PV modules offer dual functions, as a free electricity generator and a building shade or insulation envelope [44]. Previous studies utilizing univariate optimization have largely neglected the non-linear interactions arising from these dual roles, leading to suboptimal designs where supply and demand profiles are misaligned.

This paper introduces an evaluation and optimization framework of the PVAC system integrated with different BIPV types (PVAC-BIPV), focusing on dynamic energy matching by explicitly accounting for complex interactions among building parameters. Moving beyond conventional individual parameter optimization, the main contribution and novelty of the method lie in an integrated approach that builds a co-simulation framework to capture the energy interactions between BIPV modules and building envelope, then conducts a systematic, multi-parameter analysis of how orientation, shape factor, and WWR individually and synergistically affect dynamic energy matching of PVAC-BIPV systems, thereby identifying key non-linear relationships and interaction effects to establish climate-adaptive design insights.

The structure of this study is as follows: Section 2 presents the optimization framework of PVAC system integrated with different BIPV

types, establishes the model of the building, BIPV, and PVAC model considering the energy interaction between PV panels and building envelopes, and provided the real-time energy matching evaluation of the coupling system performance. Section 3 discusses the results and effectiveness of the optimization methods. Section 4 presents the conclusions.

2. Methodology

2.1. Research framework

The main motivation for research is that the energy interaction between energy generation of different BIPV types and AC energy consumption obviously impacts the real-time energy matching performance of PVAC-BIPV systems. Additionally, building design parameters, such as the orientation of walls, shape factor, and WWR, can concurrently affect both the energy generation and consumption within PVAC systems. The main purpose of this study is to increase real-time energy matching between PV generation and AC energy consumption for PVAC systems as much as possible by adopting different BIPV types, especially optimizing the PV façade design parameters. This study provides an evaluation and optimization framework for PVAC-BIPV systems integrated with different BIPV types considering the energy interactions of PVAC systems and BIPV types to improve the real-time energy matching degree for near ZEBs. The research framework is shown in Fig. 1, which can be divided into 5 steps.

In Step 1, the key design parameters affecting the real-time PV generation and AC energy consumption simultaneously were investigated by literature review, consisting of shape factor, orientation (azimuth angle), and window-to-wall ratio (WWR) of the building. Due to the large cooling demand and good consistency between PV generation and AC energy consumption in summer, two climatic regions were chosen: the hot-summer and warm-winter regions (Guangzhou) and the hot-summer and cold-winter regions (Shanghai).

In Step 2, the physical model of PVAC system integrated with different BIPV types was established by EnergyPlus software, including the model of a building, PVAC, PV roof, and PV façade. The energy interaction between the BIPV types and the building envelope was considered in the simulation.

In Step 3, a parametric study of PVAC systems with different BIPV types was conducted. The parametric simulation process was based on EnergyPlus and JePlus which can rapidly generate energy simulation results containing multiple design parameters. To determine the optimal design, the parameters mentioned above were not assigned constant values. The shape factor ranged from 0.35 to 0.55. Due to the restricted building height and building shape, the building shape factor was adjusted by changing the building's aspect ratio. In the study, both the roof area and building height were set as fixed values. Notably, with the building height maintained at 8.4 m and the roof area at approximately 300 m^2, the minimum value of shape factor was 0.355. To prevent the length-to-width ratio of the building from becoming excessively large, the maximum value of the shape factor was set at 0.555. The tilt angle of PV roof was related to the latitude of the installation location. Since most PV modules are conducted in a manner parallel to the wall, the tilt angle of PV façade was 90°. The azimuth angle ranged from 0° to 90°with increments of 15°. The WWR adjusted from 0.2 to 0.6 with increments of 0.05.

In Step 4, a comprehensive analysis of the system's energy performance was conducted. The evaluation was based on key dynamic matching indicators: solar fraction (SF), hourly self-sufficiency (SS), and hourly self-consumption (SC). Firstly, a univariate effect strength analysis was performed to quantify the individual impact of each parameter (orientation, shape factor, WWR) on the SS and SC. Subsequently, the study focused on the interaction effects between these parameters to unravel their synergistic or antagonistic influences on energy matching. Finally, the energy matching performance under various combinations of BIPV types and design parameters was comprehensively investigated across the two climatic regions.

In Step 5, the optimal design of PVAC systems integrated with different BIPV types was provided for achieving real-time energy matching in different climatic regions.

2.2. Physical model description

2.2.1. Building model

In the study, the PVAC systems were implemented in a multistory office building with dimensions of 20 m × 15 m × 8.4 m. Since the building is in the northern hemisphere, the building is determined to

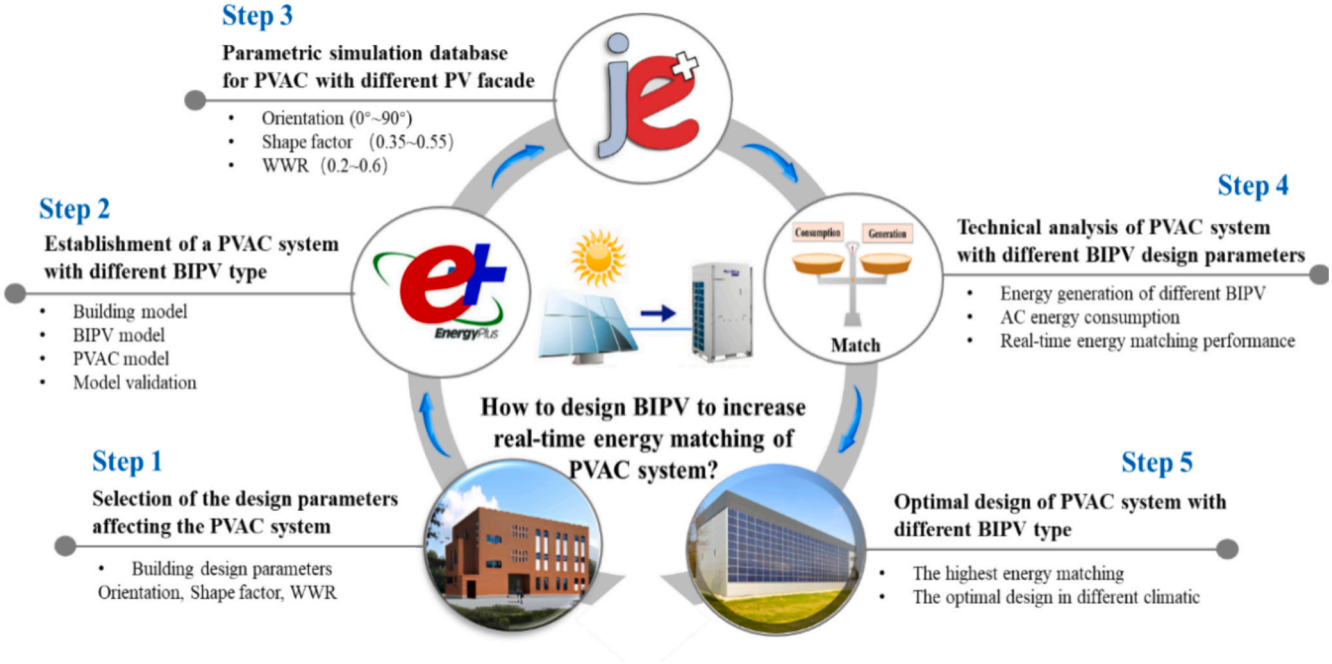


Fig. 1. The optimization framework of PVAC system with different BIPV types.

face due south (azimuth 0°), as shown in Fig. 2. Personnel, lighting, equipment parameters, and key envelope construction parameters are selected according to design standard for energy efficiency of public buildings. The heat transfer coefficients of the building envelope are shown in Table 1. The original WWR of the building is 0.35. The building is assumed to receive the maximum solar radiation without shading from the surrounding buildings.

2.2.2. BIPV model

To cover the AC energy consumption in the building, the whole BIPV system includes the PV roof system and PV façade system in Fig. 3. The PV roof system was configured with a fixed tilt angle and orientation based on the geographical location. Given the insufficient solar radiation on the northern wall, the PV modules were not installed on this surface. Therefore, the PV modules were installed on the south, west, and east exterior walls to optimize the PV generation of the building. In the simulation, these BIPV installations completely covered the south, west, and east walls, aiming to capture the maximum amount of solar energy available on these surfaces. Additionally, BIPV types of PV façade system can provide shading for building envelopes to reduce heat gain from solar radiation. Moreover, there is an air gap between the PV modules and the surface of the exterior wall to increase the PV module's performance and reduce the heat gain of buildings.

The BIPV thermal performance simulation with EnergyPlus treated the whole building with ideal air conditioning as a single zone. The south, west, and east exterior walls of the building are formed by the BIPV envelope: original exterior wall, air gap, and PV modules. The PV installed area is equal to the exterior wall area. The PV modules are installed 150 mm from the exterior wall surface [45]. The input object "Surface Property: Exterior Natural Vented Cavity" was used to model the outside boundary conditions of heat transfer with the BIPV envelope. This model uses the "Surface Property: Other Side Conditions Model" object to pass boundary conditions to the heat transfer modeling for the exterior wall surface of the building. The equivalent One-Diode model in EnergyPlus was employed to evaluate the electrical performance of BIPV systems.

2.2.3. PVAC model

In this study, a grid-connected PVAC system was selected to investigate the real-time energy matching degree in different climatic zones. The real-time electricity generated by the PV system is used to drive the air conditioning. The AC model is regarded as an ideal air conditioning system. The nominal COP is 3.99. The validity and implications of these simplifications are further examined through a dedicated sensitivity analysis in Section 3.4.Considering thermal comfort and energy-saving requirements, the indoor air temperature is set at 25°C in summer.

2.2.4. Model validation

The physical model of building and BIPV types are constructed in EnergyPlus. The simulation of PV roofs and AC energy consumption have been previously validated [11]. To validate the model of PV façade in EnergyPlus, the comparison between experimental and simulated results of PV façade was discussed. Gao et al. has tested the surface temperature of exterior wall and air temperature in the cavity [45]. In the study, the thermal performance of buildings with or without PV façade was investigated. With the same building and PV façade, the building with PV façade was modeled in EnergyPlus. To validate the accuracy of this model, the relative error (RE) was employed to quantify the deviation between experimental and simulated data, which is calculated by Eq (1):

$$RE = \left| \frac{X_{sim} - X_{exp}}{X_{exp}} \right| \quad (1)$$

Where X_{sim} is the simulated data, X_{exp} is the experimental data.

The comparison of experimental and simulated results for the PV facade is presented in Fig. 4. The maximum RE values between simulated and experimental values are 9.8% for PV integrated wall and 8.55% for the non-PV wall, both within acceptable engineering tolerance thresholds. Notably, comparative analysis revealed that non-PV wall surfaces exhibited lower RE values, with the maximum discrepancy reduced to 8.55%. This temperature differential can be attributed to the multifunctional performance of PV façade systems. The PV modules demonstrate significant solar shading effects that effectively mitigate direct solar heat gain, thereby reducing cooling load demands in buildings. Moreover, PV modules impede both the radiation heat dissipation of the building wall to the sky and the convective heat transfer with the surrounding environment, resulting in the surface temperature of the PV facade being higher.

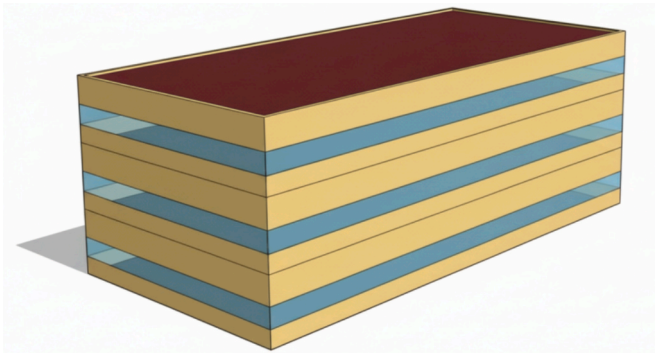


Fig. 2. The layout of the office building.

Table 1
The heat transfer coefficients (K-value) of the envelope structures.

Component (W/(m^2·K))	Building in Shanghai	Building in Guangzhou
Roof K	0.5	0.5
Exterior wall K	0.8	1.5
Exterior window K	2.6	2.8
Interior wall K	0.8	0.8
Floor K	0.8	0.8

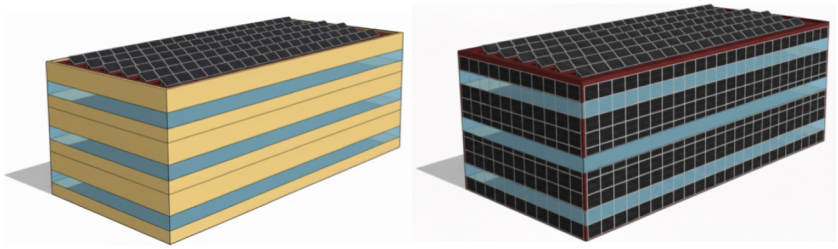
2.3. Evaluation indicators

Improving the real-time energy matching between PV generation and AC energy consumption has become increasingly crucial in recent years. To address this challenge, a real-time energy matching evaluation method of PVAC systems integrated with BIPV types was proposed to optimize the design parameters of the system, including shape factor, orientation, and WWR. Three evaluation indicators were provided to assess the energy performance of the coupling system including the solar fraction (SF), self-consumption ratio (SC), and self-sufficiency ratio (SS). The SF specifically evaluates the total energy matching of the PVAC systems integrated with various BIPV types in the building, as shown in Eq. (2). If the SF equals 1, the zero energy goal of air conditioning can be obtained through optimized BIPV-storage integration. However, the inherent intermittency of solar radiation introduces a significant real-time energy mismatching problem of the PVAC system, requiring energy storage systems with larger capacity to maintain grid independence when sunlight is limited.

$$SF = \frac{\int_{t=0}^{T} P_{pv}}{\int_{t=0}^{T} L_{ac}} \quad (2)$$

Where P_{pv} represents the hourly PV generation, Wh; L_{ac} represents the hourly AC energy consumption, Wh; T represents the operation periods.

SS indicates the probability that the PV electricity generation can directly meet the consumption requirements of the air conditioners in the operation periods, as shown in Eq. (3). SS ranges from 0 to 1. When



(a) PV roof system (b) PV façade system

Fig. 3. The layout of the office building with different BIPV types.

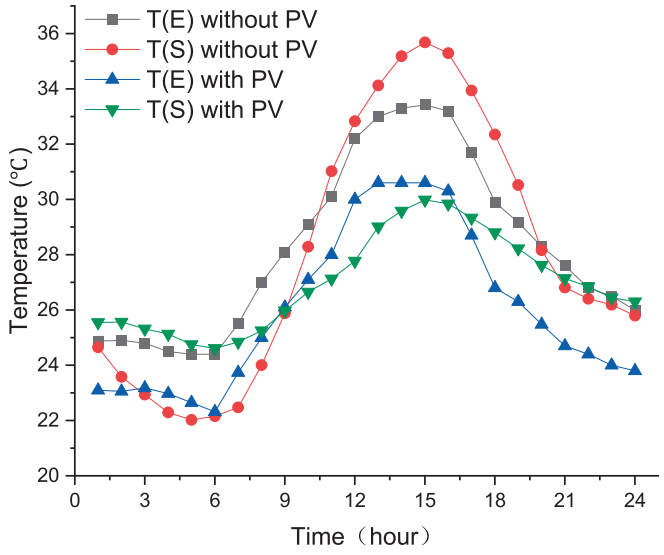


Fig. 4. The comparison of experimental and simulation data of surface temperature.

SS is less than 1, it indicates that the PV generation fails to fully meet the power consumption of the AC currently.

$$SS = \frac{\int_t^{t+1} M(t)}{\int_t^{t+1} L(t)} = \frac{\int_t^{t+1} \min(L(t), P(t))}{\int_t^{t+1} L(t)} \tag{3}$$

Where, M(t) represents the real-time overlap of PV generation and AC power consumption, W; L(t) represents the power consumption per hour of the AC system, W; P(t) represents the power generation per hour of the PV system, W.

SC indicates the effective utilization of real-time PV electricity generation and is also an important indicator to measure the degree of energy matching between PV generation and AC energy consumption, as shown in Eq. (4). The value of SC ranges from 0 to 1. When SC is equal to 1, it implies that all the PV generation during the period is consumed by the AC. When SC is less than 1, it indicates that there is an excess of PV generation during this period. This indicator can assess whether the installed capacity of the PV system is overly large.

$$SC = \frac{\int_t^{t+1} M(t)}{\int_t^{t+1} P(t)} = \frac{\int_t^{t+1} \min(L(t), P(t))}{\int_t^{t+1} P(t)} \tag{4}$$

The Mean Strength (S_{mean}) quantifying the univariate influence of a parameter x_j on the target variable y (SS or SC), is defined as the average of the absolute values of the gradient of the partial dependence function for x_j with respect to x_j.

$$S_{mean}(x_j) = \frac{1}{N}\sum_{i=1}^{N}\left|\frac{\partial \hat{f}_{x_j}(x_j)}{\partial x_j}\right| \approx \frac{1}{K\text{-}1}\sum_{k=1}^{K-1}\left|\frac{\Delta \hat{y}_{PDP}}{\Delta x_j}\right| \tag{5}$$

Where, $\hat{f}_{x_j}$ is the partial dependence function for feature x_j, where all other features have been marginalized out. The code implements this numerically by calculating the finite difference slope $\left(\frac{\Delta \hat{y}_{PDP}}{\Delta x_j}\right)$ across the grid points (K) of the partial dependence plot (PDP) curve and taking the mean absolute value. A higher mean strength value implies that the system's energy matching degree is highly sensitive to the variation of that specific parameter, indicating a steeper slope in the response curve.

3. Results and discussion

3.1. Energy performance of PVAC systems integrated with BIPV types

3.1.1. Seasonal energy performance

Given the good consistency of PV generation and AC energy consumption in summer, the energy performance of PVAC systems integrated with different BIPV types was investigated in the hot-summer cold-winter zone and the hot-summer warm-winter zone. To discuss the impact of different BIPV types on the seasonal energy matching performance, such as PV roof, south, west, and east PV facades, the solar fraction (SF) values of PVAC systems integrated with different BIPV types were calculated. This analysis aimed to clarify how different BIPV configurations enhance energy utilization of PVAC systems in different climates, particularly in summer when solar availability aligns with cooling demand.

As shown in Table 2, the SF of PVAC coupling systems exhibits significant geographic variation under different BIPV configurations. Integrated with PV roof, the SF value of the coupling system was 65.99% and 39.02% in Shanghai and Guangzhou. Then, integrated with PV roof and south PV façade, the SF value can be increased to 82.49% and 48.81%. The increment of SF is larger in Shanghai with the implementation of PV facades. Due to the higher solar radiation and lower outdoor temperature, the PV generation is higher under the same PV-installed area in Shanghai. In addition, the AC energy consumption is much lower under the same BIPV types. Therefore, the seasonal energy matching performance of PVAC systems integrated with different BIPV

Table 2
Seasonal energy performance of PVAC integrated with different BIPV types.

Energy PV surface	Energy-consumed (kWh)		Energy-generated (kWh)		SF (−)	
	SH	GZ	SH	GZ	SH	GZ
Roof	14,258	20,004	9,362	7,804	0.6566	0.3902
Roof, S facade	14,043	19,798	11,583	9,663	0.8249	0.4881
Roof, S-W facade	13,877	19,623	14,016	11,857	1.0101	0.6043
Roof, S-W-E facade	13,693	19,427	15,942	13,582	1.1642	0.6992

types is better in Shanghai (see Table 3).

As shown in Table 2, when the PV system is installed on the roof, south, and west façade, the SF is 1.01 under the existing building design parameters in Shanghai. The high SF values derive from its dual meteorological characteristics of high solar radiation and low outdoor temperature. This technical advantage enables architects to modify design parameters to balance function with aesthetic appeal of a building, without being strictly constrained by the requirements for building energy conservation. This contrasts sharply with Guangzhou's maximum SF of 69.92% even with four-surface PV deployment, revealing fundamental climate constraints. In Guangzhou, it is essential to reduce the building load demand and increase the installed PV capacity through the variation of building design parameters, such as decreasing WWR, changing shape factor and orientation of the building.

Among different PV facades, west PV façade demonstrates superior SF enhancement capabilities across both climatic regions. The increment of SF is 18.51% and 11.62% by implementing west PV façade in Shanghai and Guangzhou, respectively. However, the increment of SF is only 16.83% and 9.79% by implementing south PV facade in the two regions. Notably, the installation area of west PV façade is only 75% of south PV façade. The main reason is that the temporal synchronization of peak PV generation of west facade and peak AC energy consumption is much higher. In addition, the west façades exhibit the highest incident solar radiation in Shanghai and Guangzhou, which contributes to the highest SF increment. This phenomenon accentuates the pivotal role played by the optimization of diverse PV facades in building design for a higher energy matching degree.

While seasonal energy matching establishes theoretical performance benchmarks of PVAC coupling systems, it does not imply a high real-time energy matching level. The critical temporal resolution gap between aggregate seasonal matching and instantaneous consumption and generation alignment persists as a fundamental challenge. Absent an effective design method to increase real-time energy matching, the PVAC integrated with BIPV types may still heavily rely on the utility grid or batteries to achieve real-time energy matching. Furthermore, the augmentation of PV façade may exacerbate the burden on the utility grid or require a larger battery capacity.

3.1.2. Dynamic energy matching performance

From the real-time energy matching performance of PVAC integrated with different BIPV types, PV facades with different orientations affect the PV generation and change the building load demand. Given that the areas of various facades are different, the hourly energy generation per area of PV facades and AC energy consumption per area were calculated. As shown in Fig. 5, in terms of real-time energy generation of the PV roof and AC energy consumption, the PV roof exhibits significant limitations. The peak PV roof generation may occur 2–3 h earlier than the maximum AC energy consumption in the afternoon. The temporal consistency between the PV roof generation and AC energy consumption is not high. Moreover, restricted by the limited roof area, the capacity of the PV roof remains relatively small. Consequently, in the scenario where only PV roof generation is employed to operate air conditioning, two major issues emerge. Firstly, there is a substantial gap between total PV generation and AC energy consumption in the building. Secondly, the real-time energy matching degree is rather poor at many moments during the day. Compared with the PV roof, PV facades with different orientations exhibit varying PV generation trends and larger total PV generation. A higher real-time energy matching degree can be obtained by effective combination and optimization of PV façades.

Table 3
Dynamic energy performance of PVAC integrated with different BIPV types.

Energy PV surface	Self-Sufficiency (SS)		Self-Consumption (SC)	
	SH	GZ	SH	GZ
Roof	0.4154	0.2752	0.6327	0.7053
Roof, S facade	0.4862	0.3394	0.5894	0.6953
Roof, S-W facade	0.5782	0.4128	0.5724	0.6831
Roof, S-W-E facade	0.6255	0.4691	0.5373	0.6709

Among PV facades with different orientations, south PV facades remain prevalent in northern hemisphere BIPV design due to their superior annual irradiance capture. Since PV roofs are commonly oriented to face south, the PV generation trends of PV roofs and south PV facades are similar. However, the generation of the south PV façade is relatively lower. The main reason is that, even when oriented southward, vertical surfaces receive less incident radiation than optimally inclined PV roof, as depicted in Fig. 6. Compared with south PV facades, the generation of west and east PV facades is higher. There are pronounced distinctions in the variation trends of their power generation. For the east PV façades, the generation curve often reaches its peak in the morning and remains at a relatively low value in the afternoon. In contrast, the power generation of west PV facades is generally low in the morning but peaks in the afternoon. The generation diversification of different PV facades achieves dual benefits. It not only cuts down AC energy consumption but also provides more diversified and variable power resources. Therefore, the application of PV facades serves as an effective method to achieve real-time energy matching for PVAC systems.

In Guangzhou, the SS of PVAC systems integrated with PV roofs is only 27.52%. The normal operation of PVAC systems should be heavily reliant on the utility grid. Compared with Shanghai, the PV generation is lower with the same PV roof system in Guangzhou due to the lower solar radiation. The AC energy consumption is much greater than that in Shanghai. This phenomenon results in a much lower SS and higher SC under the same coupling system of PVAC and PV roof. With south, west, and east PV facades in Guangzhou, the SS value can be increased by 6.42%, 7.34%, and 5.63% respectively, while the SC value can be reduced by 1.0%, 1.22%, and 1.22% respectively.

In general, from the impact of PV facades with different orientations on the energy matching of PVAC systems in two regions, the improvement rates of SS with south PV facades are 7.08% and 6.42% in Shanghai and Guangzhou respectively, both of which are lower than that with west walls. In both regions, due to severe westward solar exposure of buildings in summer, west PV facades can more effectively reduce the load demand and increase PV generation, thus enhancing the real-time energy matching of PVAC systems, followed by the south and east facades. Overall, the PV facades can significantly influence the real-time energy matching degree. The optimization of building design parameters to change PV facades is important to improve the real-time energy matching of PVAC systems.

3.2. Effect strength analysis of design parameters

Building orientation (azimuth angle), shape factor (F), and window-to-wall ratio (WWR) are the main factors influencing AC energy consumption and PV installed capacity simultaneously. In this paper, with dynamic energy matching as the optimization objective and taking shape factor, azimuth angle, and WWR as variables, an optimization method was explored for PVAC systems integrated with different BIPV types. Firstly, the dynamic energy matching performance of PVAC systems integrated with different BIPV types was investigated with varying shape factors, azimuth angles, and WWR values. Secondly, the optimized design parameters were obtained by maximizing SS values and SF values in different climatic regions. Finally, based on the impact of parameter variations on the real time energy matching of the coupling system, the order of importance of different parameters was obtained.

3.2.1. Univariate effect strength analysis of individual parameters

To assess the impact of key design parameters on system energy performance, a univariate effect strength analysis was conducted in Guangzhou and Shanghai. The univariate effect strength refers to the average marginal impact intensity of a single parameter on the target variable (SS or SC) when other parameters are kept constant. This

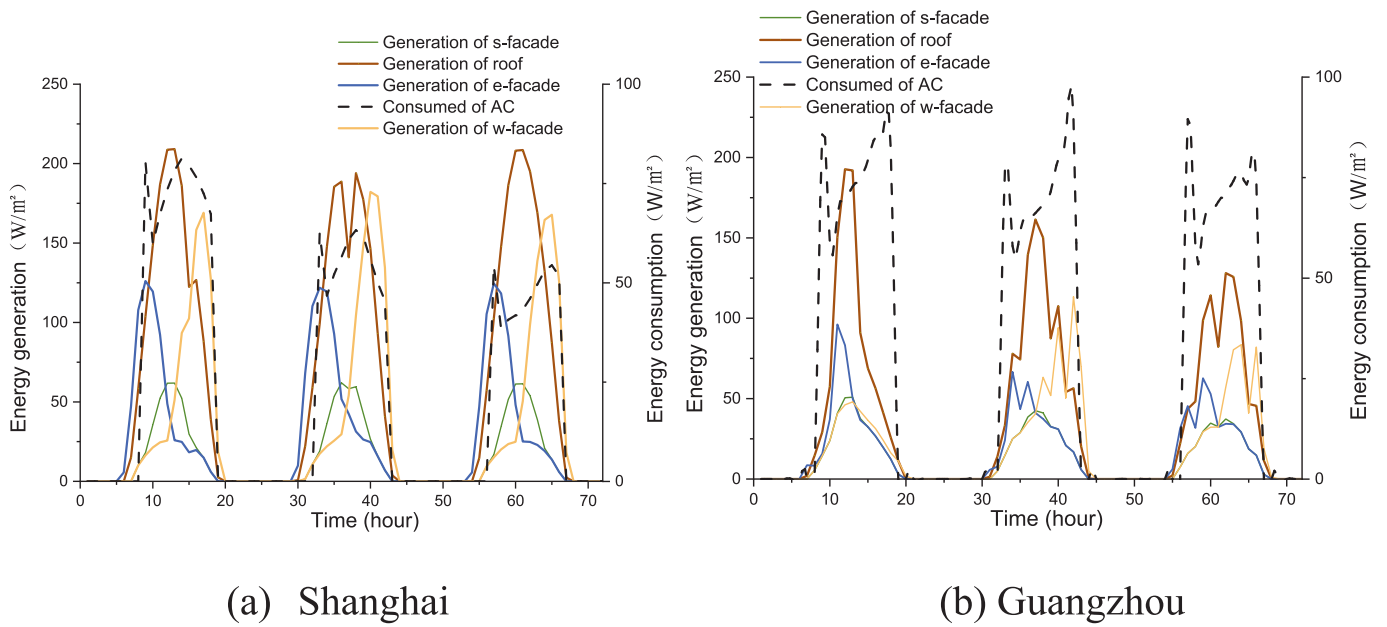


Fig. 5. The real-time energy generation and consumption of PVAC systems in different regions.

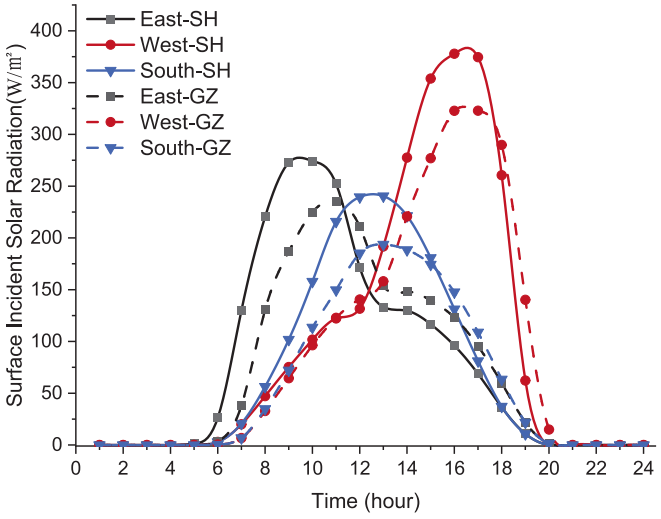


Fig. 6. The incident solar radiation of different building surfaces in different regions.

indicator helps identify the dominant parameters governing system's energy balance, as well as the differentiation of parameter sensitivity levels. The results for PV-integrated buildings in each region are summarized in in Table 4.

As shown in Table 4, the shape factor exhibits the highest mean strength of 5.38 in Guangzhou and 2.90 in Shanghai, identifying it as the dominant driver for energy matching. A 10% variation in the shape factor results in an approximately 10.8% fluctuation in the SS value in Guangzhou, underscoring its pivotal role. The dominance of the Shape Factor stems from its role in determining the building's surface-to-volume ratio. Unlike WWR, which only reallocates the proportion of glazing on a fixed façade, the shape factor scales the total envelope area. An increase in the shape factor, driven by the variation of the building aspect ratio under constant volume constraints, simultaneously expands the PV installation capacity on the supply side and the external heat transfer surface on the demand side. This dual amplification mechanism causes the energy matching indicators to fluctuate more drastically per unit change in the shape factor compared to other parameters.

Table 4
The univariate effect strength of different parameters.

Region	Parameter	Indicators	Mean Strength	Variation
Guangzhou	Shape factor	SS	5.38	10.8%
		SC	2.91	5.8%
	WWR	SS	0.33	1.3%
		SC	0.15	0.6%
	Orientation	SS	0.03	0.3%
		SC	0.05	0.5%
Shanghai	Shape factor	SS	2.90	5.8%
		SC	1.37	2.7%
	WWR	SS	0.21	0.9%
		SC	0.25	1.0%
	Orientation	SS	0.05	0.5%
		SC	0.06	0.6%

Furthermore, the significantly higher mean strength observed in Guangzhou compared to Shanghai is attributed to the climatic disparity. In the hot-summer and warm-winter zone of Guangzhou, the intense solar radiation and higher ambient temperatures mean that any increase in the envelope surface area incurs a much more severe penalty in solar heat gain. Consequently, the cooling load dominates the energy balance equation more aggressively in Guangzhou, making the system far more sensitive to geometric variations than in the milder climate of Shanghai.

In contrast to the global influence of the shape factor, the Window-to-Wall Ratio (WWR) exhibits a comparatively subordinate univariate effect, with a mean strength of only 0.33 for SS in Guangzhou. Physically, this disparity stems from the fact that the shape factor determines the total surface magnitude of the building envelope, whereas the WWR functions primarily as an allocative parameter within these fixed boundaries. A reduced ratio yields a synergistic advantage by expanding the opaque wall area available for PV generation on the supply side while concurrently minimizing the transparent glazing area responsible for solar heat gain on the demand side. Although this simultaneous optimization effectively improves the self-sufficiency ratio, the extent of this improvement is structurally constrained by the finite total façade area. Consequently, the Window-to-Wall Ratio serves as a secondary adjustment variable relative to the foundational scaling effect of the Shape Factor.

Building orientation exhibits the lowest mean strength, with values

ranging from 0.03 to 0.06. Unlike shape factor or WWR, which fundamentally alter the total energy magnitudes by scaling available surface areas, orientation primarily governs the temporal energy distribution. An optimal orientation enhances real-time energy matching by synchronizing peak PV generation with peak cooling demand. However, the Mean Strength indicator averages the parameter's impact over the entire seasonal period. Since building orientation primarily redistributes the diurnal profile of incident solar radiation rather than altering its total daily integral, the cumulative impact on the aggregated seasonal energy balance remains limited. In contrast, capacity-oriented parameters like Shape Factor and WWR directly reduce the total thermal load and increase the total generation capacity, leading to a much larger cumulative impact on seasonal performance metrics.

For SC value, while the rank order of parametric influence remains identical, its sensitivity to design changes is consistently less pronounced than that of SS. For instance, the mean strength of shape factor for SC is only 2.91 in Guangzhou, compared to 5.38 for SS. This disparity is fundamentally attributed to the different denominators used in their definitions and their distinct responses to geometric variations. For SS, its denominator (L_{total}) fluctuates aggressively with building parameter changes, causing the ratio to exhibit high responsiveness. For SC, the denominator (P_{total}) scales more predictably with envelope area than the complex thermal load does. As capacity-oriented parameters like shape factor are adjusted, they tend to influence both the matched energy and the total PV generation in a synchronized manner. This concurrent movement creates a mathematical damping effect, mitigating the overall fluctuation in the SC ratio. Consequently, while both SS and SC are valuable metrics, SS serves as a more sensitive indicator for evaluating architectural design strategies aimed at improving energy matching, whereas SC is more indicative of the system's overall PV utilization efficiency. This distinction provides an essential insight for prioritizing design interventions.

In Shanghai, the rank order of parametric influence based on Mean Strength values remains identical to that of Guangzhou, with shape factor exerting the strongest effect, followed by WWR and orientation. However, the Mean Strength values for shape factor and WWR are consistently lower. The main reason is the different baseline energy performance of PV-integrated buildings in Guangzhou and Shanghai. In Shanghai, the load demand is smaller and PV generation is higher with identical building design, resulting in a higher SS value. In Guangzhou, the system with higher load demand and lower PV generation starts from a lower SS baseline. This means that the parametric optimization has a greater potential to markedly to improve the system's energy matching.

3.2.2. *Interaction effect strength analysis of parameter combinations*

While univariate analysis clarifies the independent impacts of each parameter, this study further examined the interaction effects between parameters on system energy performance. The interaction effect mean strength of key parameter combinations on system's performance were shown in Table 5. To ensure clarity in the following analysis, the key design parameters are abbreviated as follows: Shape Factor (S), Window-to-Wall Ratio (W), and Orientation (O). In this table, the mean strength of parameter combination specifically refers to the average intensity of the addiction impact on system's energy performance arising from the synergistic variation of two parameters.

Among all combinations, the interaction between shape factor and WWR (S × W) consistently exhibits the highest mean strength for SS value. With values reaching 0.0491 in Guangzhou and 0.0326 in Shanghai, this pairing is established as the dominant synergistic driver for optimization. This dominance is rooted in a powerful synergistic and amplifying mechanism between the two parameters. The shape factor determines the total envelope area, which in turn acts as a geometric scaling factor that amplifies the thermal and electrical consequences of any change in WWR. Consequently, this multiplicative coupling renders the synergistic adjustment of Shape Factor and WWR the most critical lever for performance optimization

Table 5
The interaction effect strength of different parameters.

Region	Parameter Combination	Indicators	Mean Strength
Guangzhou	S × W	SS	0.0491
	S × W	SC	0.0235
	S × O	SS	0.0336
	S × O	SC	0.0199
	O × W	SS	0.0386
	O × W	SC	0.0219
Shanghai	S × W	SS	0.0326
	S × W	SC	0.0344
	S × O	SS	0.0262
	S × O	SC	0.0236
	O × W	SS	0.0279
	O × W	SC	0.0320

Note: S denotes Shape Factor; W denotes Window-to-Wall Ratio; O denotes Orientation. The notation S × W, etc., represents the statistical interaction effect between parameters (i.e., their synergistic or antagonistic joint influence), not their mathematical product.

The interactions involving orientation, such as orientation with WWR and orientation with shape factor, demonstrate a weaker but still significant influence. In Guangzhou, the O × W interaction exhibits a notable effect on SS, with a mean interaction strength of 0.0386. The mean interaction strength of the S × O interaction is 0.0336, which is lower than that of O × W interaction on SS. This suggest that coordinating the timing of solar gains through optimized building orientation with the WWR of the same façade yields a stronger interaction effect. This is attributed to the synergistic alignment of these two factors with the core operational demands of BIPV systems, which prioritize maximizing solar radiation capture efficiency while achieving dynamic matching between PV generation and load demand. The S × O interaction involves an inherent fundamental contradiction, which manifests in that expanding the building's surface area tends to generate additional façades with suboptimal solar orientations, thereby undermining the overall performance improvement.

As shown in Table 5, the interaction effects for SC values are generally less pronounced than those for the SS, especially in Guangzhou. For instance, the mean strength of the dominant S × W interaction for SC is only 0.0235, less than half of the corresponding 0.0491 for SS. This reduced sensitivity stems from the mathematical damping effect inherent in the definition of SC. Building parameters optimization tends to lead to simultaneous changes in M(t) and $P_{total,}$ thereby attenuating the sensitivity of SC to the synergistic and constraining effects.

Conversely, Shanghai exhibits a region-specific divergence where the mean strength of the S × W interaction for SC, at 0.0344, marginally surpasses that for SS at 0.0326. This inversion stems from the specific climatic characteristics of Shanghai, which features higher solar irradiance intensity yet milder cooling demands compared to Guangzhou. This combination creates a scenario of pronounced PV oversupply. When the building envelope expands by the S × W interaction, the high irradiance leads to a disproportionate surge in total PV generation capacity Due to the limited cooling load, the matched energy M quickly reaches its utilization limit. Consequently, the SC becomes more sensitive to the parameter variation, as the denominator P_{total} grows significantly faster than stagnant numerator M. In contrast, the SS experiences diminishing returns, rendering it less sensitive to further geometric expansion compared to SC.

Finally, a clear regional pattern is evident where interaction strengths are consistently more pronounced in Guangzhou than in Shanghai.. For the dominant S × W interaction on SS, the Mean Strength in Guangzhou is 0.0491, a value over 50% higher than the 0.0326 recorded in Shanghai. This underscores that an integrated multi-parameter optimization approach is particularly critical for climates with higher cooling demands, as these systems are inherently more

responsive to geometric design adjustments.

3.3. Optimization of PV-integrated buildings

3.3.1. Shape factor and WWR optimization

Based on the fixed azimuth angle, the dynamic energy performance of PV-integrated buildings under different shape factors and WWRs were investigated. Figs. 7–10 illustrate the dynamic energy performance under a fixed azimuth. The horizontal axis displays 25 simulation cases generated by combinatorially varying 5 shape factors and 5 WWRs. The cases are grouped by shape factor. Specifically, Cases 1 through 5 correspond to the minimum shape factor of 0.355 interacting with WWRs increasing from 0.2 to 0.6. This grouping logic repeats incrementally for subsequent Shape Factors (details in Appendix A, Table A1). The vertical axis denotes the real-time energy matching indicators.

A consistent and dominant trend observed across all scenarios is the monotonic decline in SS with increasing WWR. For instance, in Guangzhou under a fixed 0° orientation, the SS increments attributed to geometric optimization gradually decrease from 9.92% to 6.26% as the WWR increases from 0.2 to 0.6. This deteriorating trend is even more pronounced under an optimized 45° orientation, where the improvement in SS drops from 12.6% to 6.12% across the same WWR range. This is governed by a pronounced degradation in the supply–demand energy balance. On the demand side, a larger transparent area significantly intensifies solar heat gain, thereby escalating the building's cooling load. On the supply side, the expanding WWR reduces the available opaque façade area for PV installation. This compound mechanism of amplified demand and diminished supply potential renders the Window-to-Wall Ratio a highly sensitive parameter in governing the system's energy matching performance.

In contrast, the relationship between the shape factor and SS is non-linear and non-monotonic, where SS values first decrease and then increase as the shape factor rises. This non-linear behavior is driven by a fundamental trade-off inherent in the Surface-to-Volume Ratio (S/V). As the Shape Factor increases, the building becomes less compact, which simultaneously expands the total envelope area. Initially, the detrimental effect of increased thermal load from this larger surface outweighs the benefit of the expanded PV installation area, causing SS to decline. However, beyond a critical threshold, the substantial gain in PV generation capacity begins to dominate the energy balance, leading to a recovery in SS. This finding underscores that an optimal intermediate geometry exists, demonstrating that a simplistic strategy of merely minimizing or maximizing the shape factor is insufficient for achieving optimal energy matching.

A comparative analysis between Guangzhou and Shanghai reveals that while the qualitative trends are similar, the quantitative impacts differ significantly. The system in Guangzhou consistently exhibits a much stronger sensitivity to building parameters. This regional disparity is clearly evidenced by the impact of the WWR. In Shanghai, the SS increments show a relatively stable negative correlation with WWR, fluctuating within a narrow band between −12.47% and −14.17% at a 45° orientation under identical parametric variations. In Guangzhou, the regulatory range of SS resulting from the synergistic variation of shape factor and WWR demonstrates remarkable discrepancies across different building orientations. The synergistic variation of shape factor and WWR in Guangzhou yields a maximum SS improvement of 33.58% at a 45° orientation, significantly larger than the 24.21% achieved in Shanghai. This disparity is attributed to the different energy performance baselines. The system in Guangzhou operates from a lower baseline SS due to its harsher cooling demands, meaning that any geometric optimization yields a steeper marginal benefit. This highlights that an integrated design approach focusing on building design holds greater potential in climates with more extreme thermal loads.

3.3.2. Shape factor and orientation optimization

Based on the fixed WWR, the dynamic energy performance of PV-integrated buildings under different shape factors and WWRs were investigated in detail. As shown in Figs. 11–14, the case number, ranges from 1 to 35. These cases are generated by combining 5 building shape factors and 7 orientations. Specifically, Cases 1 through 7 correspond to the minimum Shape Factor of 0.355 interacting with orientations from 0° to 90° in 15° increments, while Cases 8 through 14 correspond to the second Shape Factor of 0.360, and so forth.

Compared with the SS variation with increasing WWR, the SS value demonstrates a characteristic non-monotonic relationship with building orientation, initially rising then declining with increasing azimuth angle. This behavior results from temporal synchronization between PV generation and the building's cooling load profile. In Guangzhou, the system achieves a maximum SS value of 76.22% with a shape factor of 0.555, WWR of 0.2, and orientation of 45°, while the SC value reaches 49.27%. While south-facing façades receive high total irradiation, west-facing façades experience peak irradiance in the late afternoon, which better aligns with the typical peak cooling demand of office buildings. An intermediate orientation, such as 45°, achieves a synergistic balance between the high generation potential of south-facing surfaces and the superior temporal alignment of west-facing surfaces, thereby maximizing real-time energy matching. However, rotating the building beyond this optimal angle leads to a rapid decline in SS, as the reduction in total generation from the prime south-facing surfaces begins to dominate the energy balance.

The shape factor significantly modulates this orientation sensitivity. A larger shape factor increases the building's aspect ratio, thereby amplifying the surface area of specific façades such as the East and West

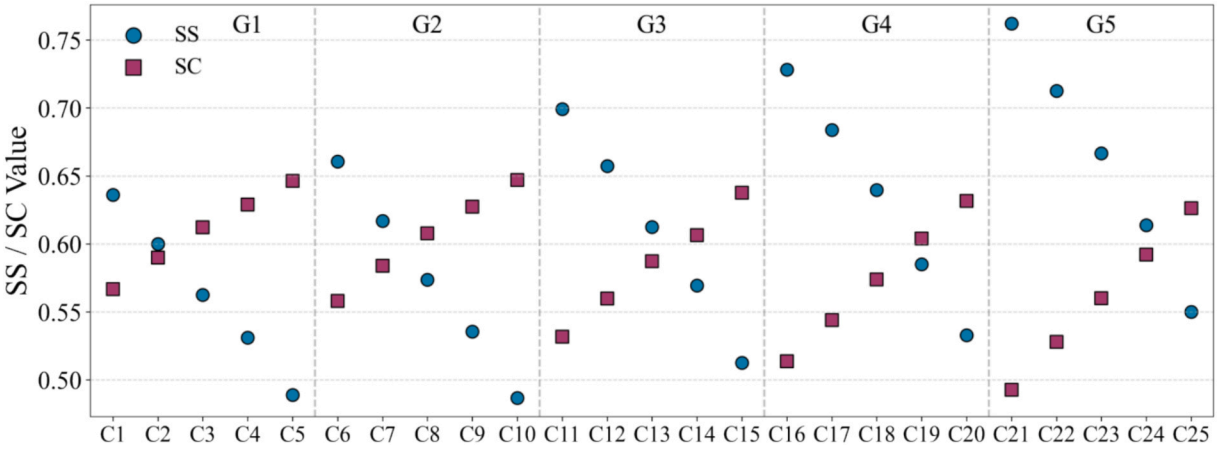


Fig. 7. The energy matching of PVAC systems with different shape factors and WWR in Guangzhou (O = 45°).

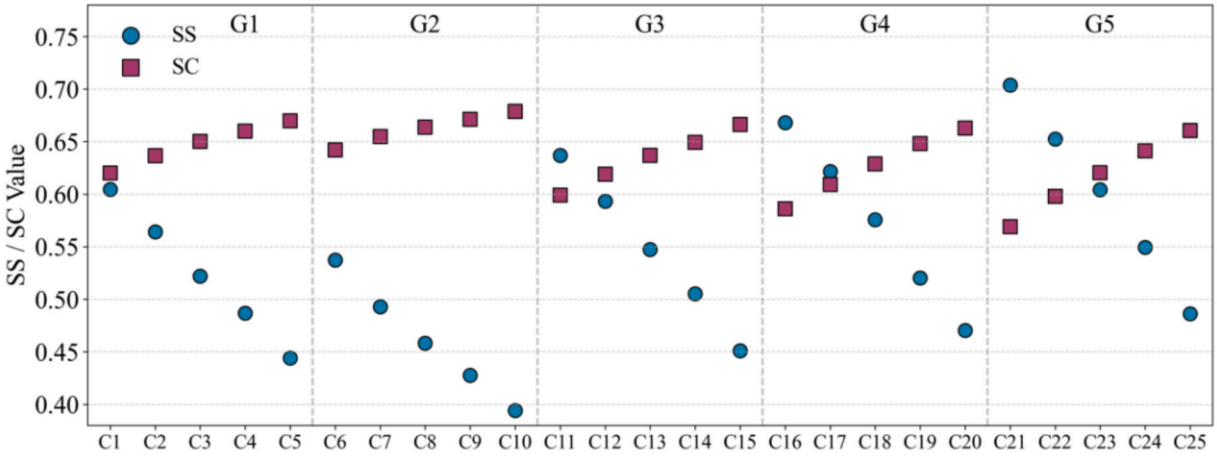


Fig. 8. The energy matching of PVAC systems with different shape factors and WWR in Guangzhou (O = 0°).

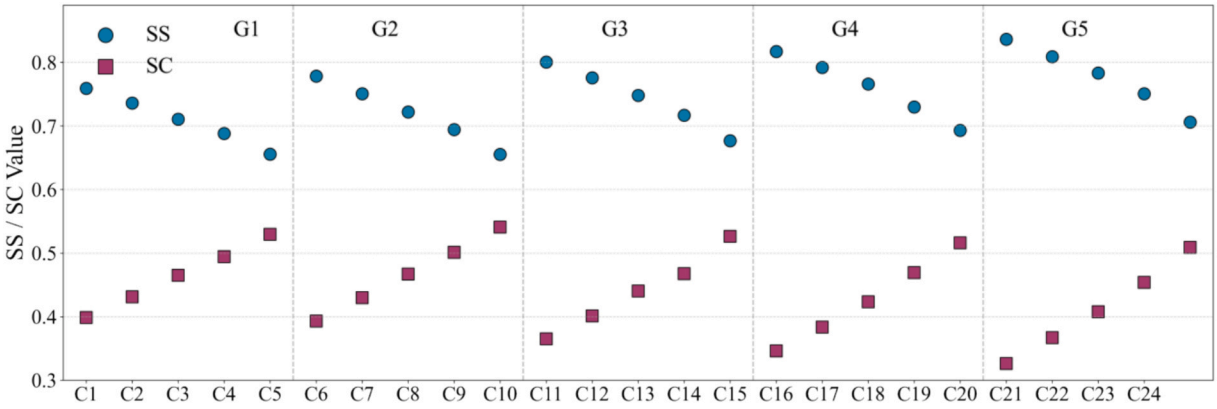


Fig. 9. The energy matching of PVAC systems with different shape factors and WWR in Shanghai (O = 45).

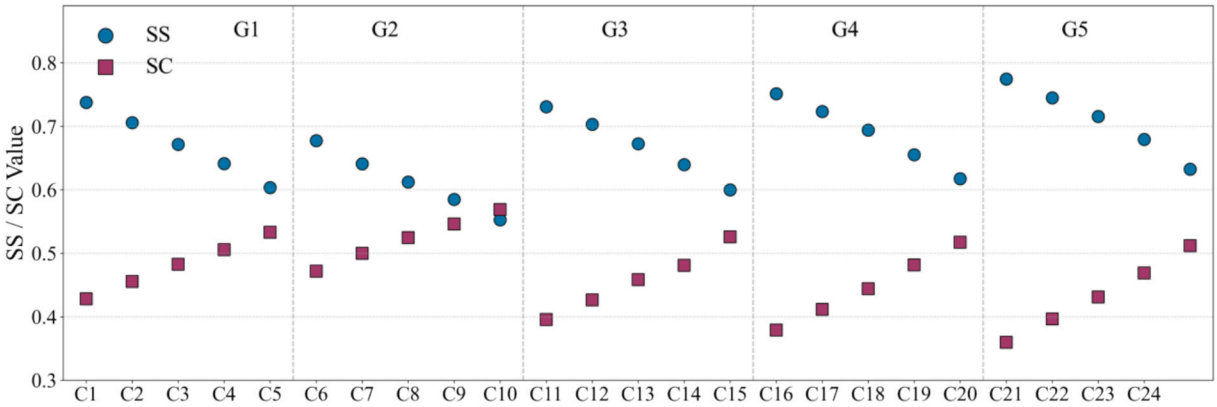


Fig. 10. The real-time energy matching of PVAC systems with different shape factors and WWR in Shanghai (O = 0).

walls. This interaction means that the benefit of optimizing orientation is magnified in buildings with larger shape factors. In Guangzhou, with a WWR of 0.2, the benefit of optimizing orientation is particularly pronounced for buildings with a large Shape Factor. For a Shape Factor of 0.555, shifting the orientation from 0° to the optimal 45° increases the SS value substantially, from approximately 0.63 to 0.76. In contrast, the improvement for a compact shape factor of 0.355 is considerably less pronounced. This data confirms that elongated buildings provide a larger façade area, increasing the potential to optimize energy performance by aligning these surfaces with favorable solar orientations. This proves that the optimal orientation can shift depending on the building design and highlights the necessity of multi-parameter co-optimization.

A comparative analysis reveals that the system in Shanghai consistently exhibits superior performance, achieving a peak SS of 83.61% under the same parametric configuration that yields only 76.22% in Guangzhou. Furthermore, the SS in Shanghai demonstrates a wider fluctuation range and stronger non-linear characteristics in response to orientation changes. This heightened sensitivity is primarily attributable to the higher and more variable direct solar irradiance in Shanghai. This climatic feature makes the PV generation profile highly responsive to

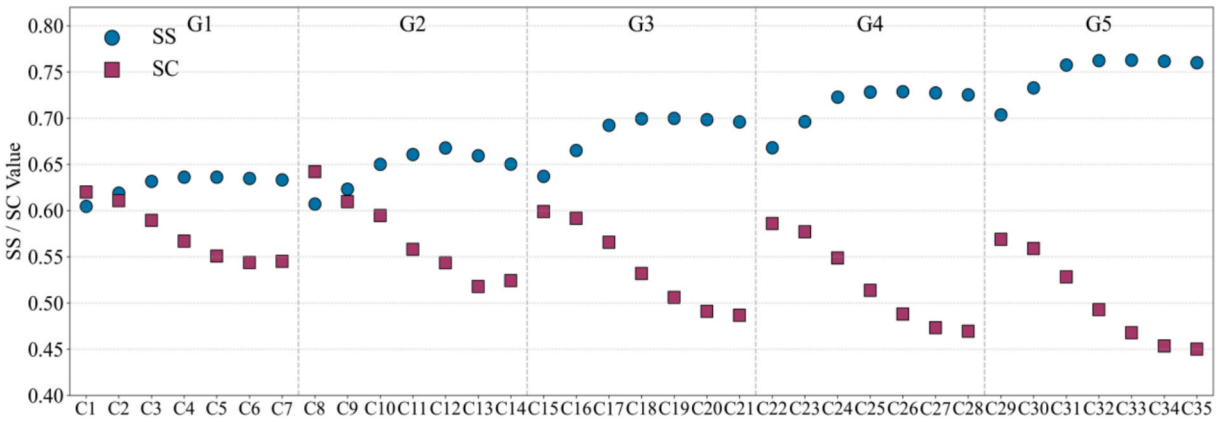


Fig. 11. The dynamic energy matching of PVAC systems with different shape factors and Orientation in Guangzhou (WWR = 0.2).

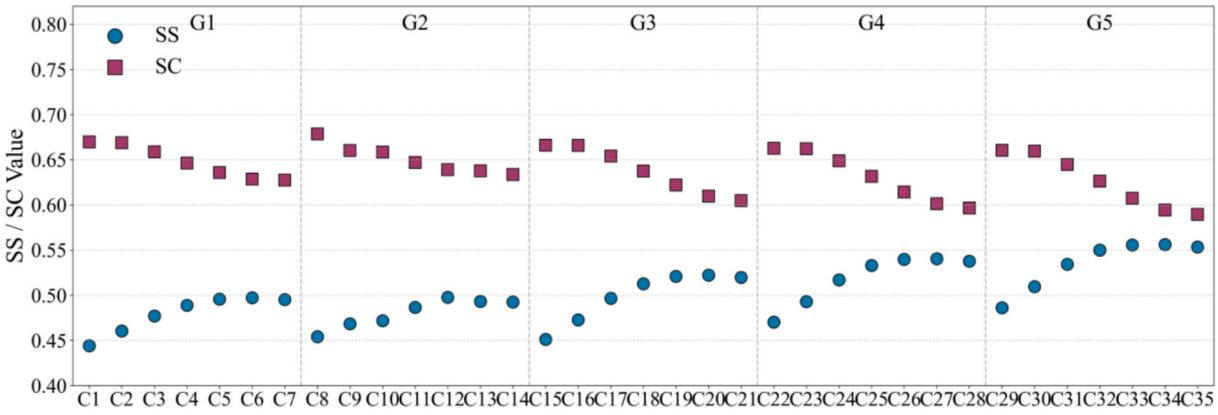


Fig. 12. The dynamic energy matching of PVAC systems with different shape factors and Orientation in Guangzhou (WWR = 0.6).

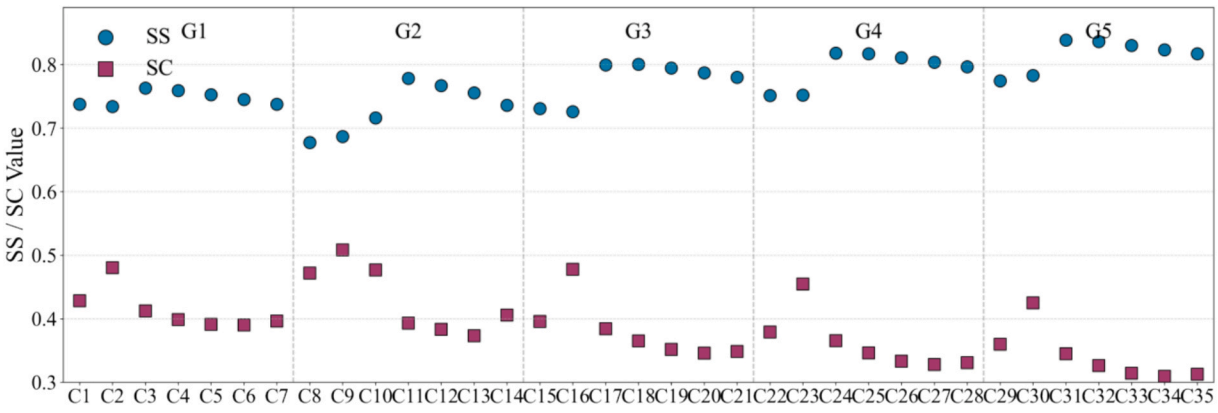


Fig. 13. The dynamic energy matching of PVAC systems with different shape factors and Orientation in Shanghai (WWR = 0.2).

azimuth changes, which necessitates a more precise orientation alignment to match the load demand. Consequently, this heightened sensitivity creates a greater potential for performance improvement through synergistic parameter design.

3.3.3. *Orientation and WWR optimization*

The interaction between Orientation and WWR is presented in Figs. 15–18. The 35 cases represent the cross-combination of 7 Orientations and 5 WWRs. To facilitate analysis, the data is organized by Orientation groups. Cases 1 through 5 represent the South orientation (0°) with WWR increasing from 0.2 to 0.6, while Cases 6 through 10 represent the 15° orientation, continuing sequentially up to the West orientation (90°).

As shown in Figs. 15–18, regardless of the influence exerted by Orientation or Shape Factor, the SS value exhibits a consistent downward trend with the increase in WWR, while the SC value demonstrates a steady upward trend as WWR rises. It is obvious that the WWR is the dominant factor within this interaction.

While the WWR trend is dominant, the magnitude of these variations reveals the comparative strength of different interactions. In Guangzhou, fixing the orientation and varying the Shape Factor and WWR produces a substantial SS variation range of 30.96%. In contrast, fixing

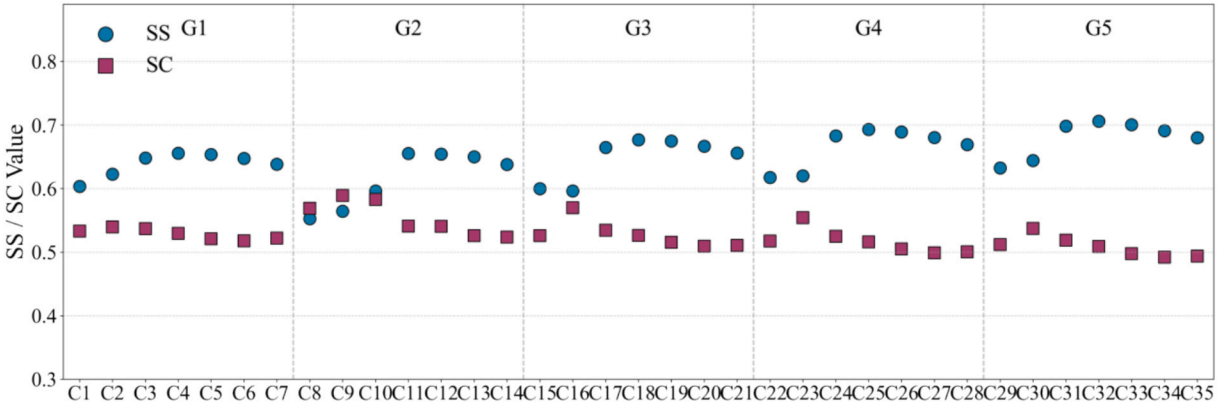


Fig. 14. The real-time energy matching of PVAC systems with different shape factors and Orientation in Shanghai (WWR = 0.6).

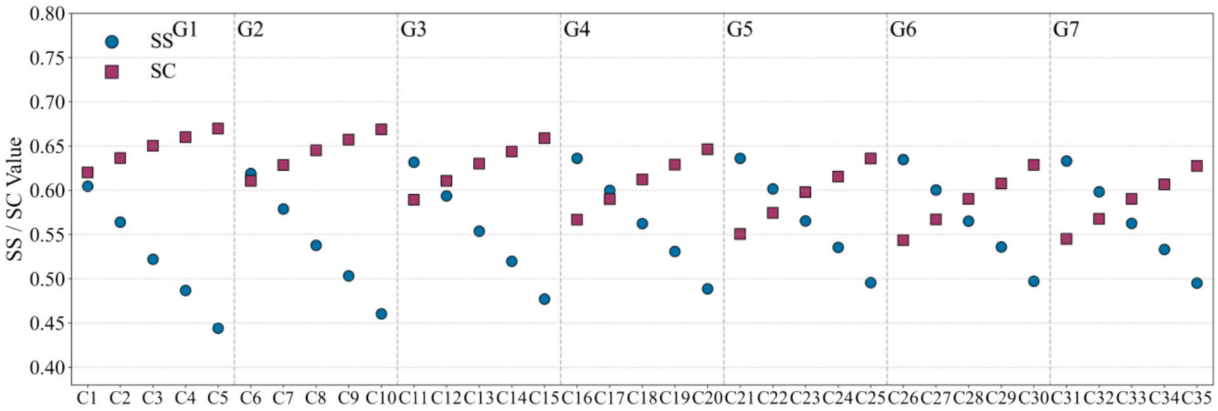


Fig. 15. The real-time energy matching of PVAC systems with different WWR and Orientation in Guangzhou (shape factor = 0.35).

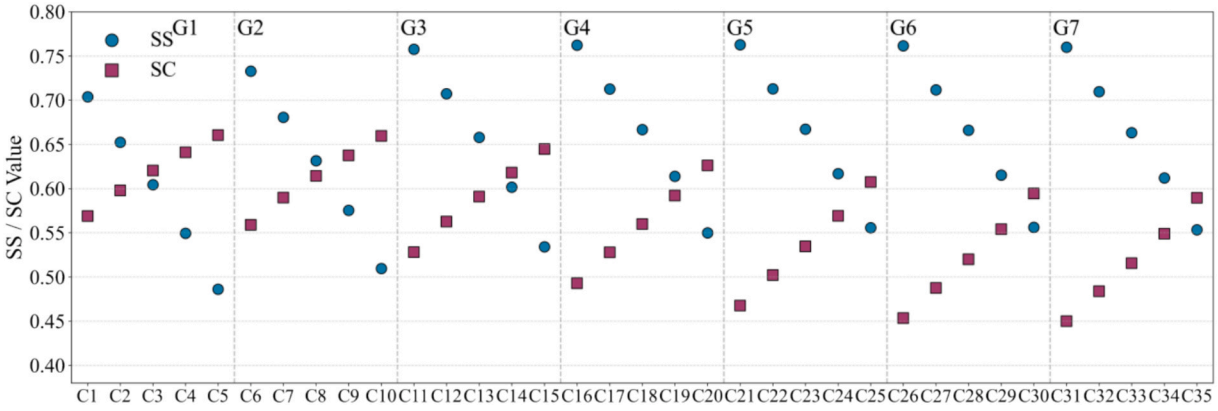


Fig. 16. The real-time energy matching of PVAC systems with different WWR and Orientation in Guangzhou (shape factor = 0.55).

the Shape Factor and varying the Orientation and WWR yields a smaller, yet still significant, variation of 19.2%. This result reveals a critical hierarchy in design influence. The interaction between WWR and Shape Factor is stronger because both parameters fundamentally govern the magnitude of energy variation. By scaling the building's area distribution, they set the upper and lower bounds for both real-time heat gain and PV generation at any given moment. In contrast, the WWR × Orientation interaction is comparatively weaker. While orientation is crucial for optimizing the temporal energy alignment by shifting the peaks and valleys of supply to better match demand, it operates within the capacity constraints already established by the building's geometry. Therefore, the building's geometry, which dictates the fundamental generation capacity and load demand, imposes a more primary constraint on the potential for real-time energy matching than does the temporal alignment of those energy flows.

A comparative analysis reveals that Shanghai demonstrates a smaller potential for improvement due to its higher baseline SS. The synergistic multi-parameter optimization yields distinct, climate-adaptive design solutions. In Shanghai, the optimal parameter set of 45° orientation, 0.555 shape factor, and 0.2 WWR achieves a peak SS value of 83.84%. In Guangzhou, the optimal combination shifts to 60° orientation, 0.555 shape factor, and 0.2 WWR, resulting in a maximum SS of 76.26%. The substantial optimization range observed in both regions, with minimum SS values dropping as low as 34.32% in Guangzhou, highlights the

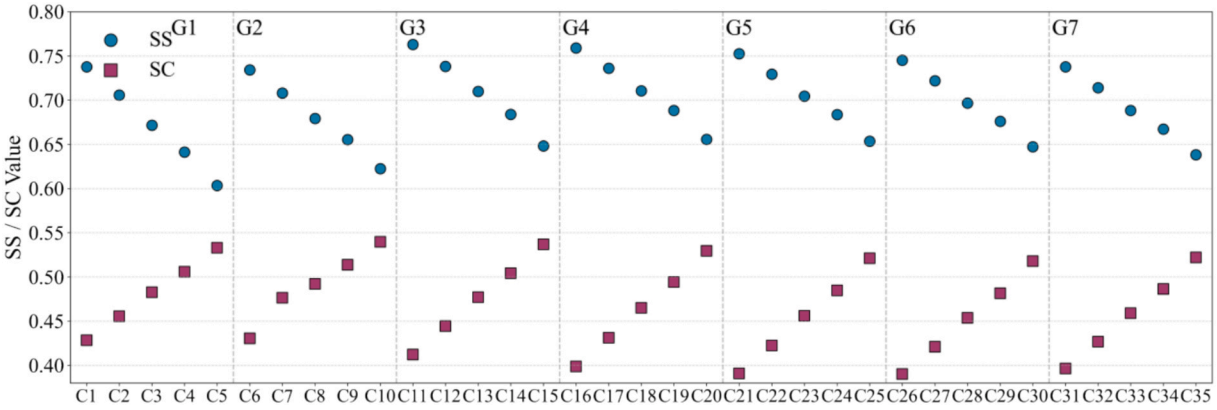


Fig. 17. The real-time energy matching of PVAC systems with different WWR and Orientation in Shanghai (shape factor = 0.35).

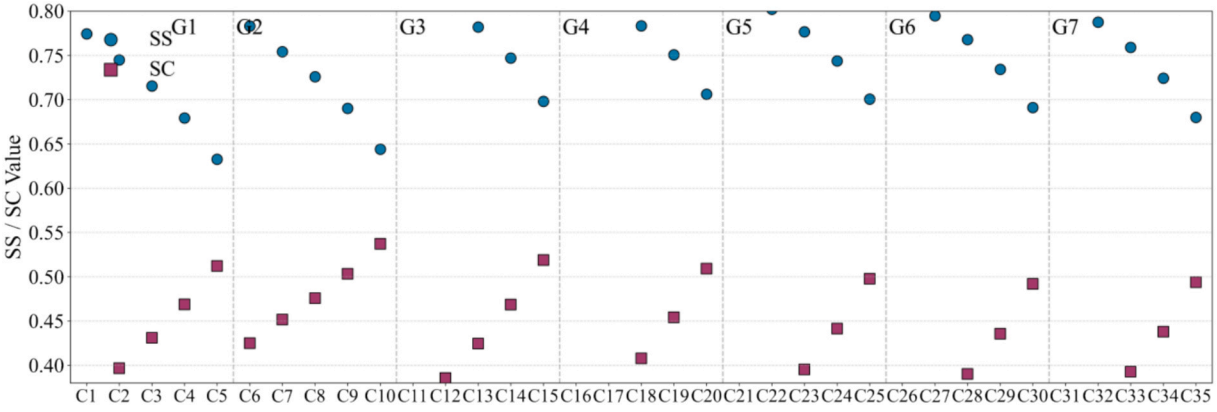


Fig. 18. The real-time energy matching of PVAC systems with different WWR and Orientation in Shanghai (shape factor = 0.55).

critical necessity of a holistic, multi-parameter co-optimization approach for designing high-performance PV-integrated buildings.

In summary, while a low WWR and a large shape factor are universally beneficial, the optimal orientation is highly climate-dependent. The 60° optimum in Guangzhou prioritizes alignment with intense afternoon solar radiation to meet higher cooling loads, whereas the 45° optimum in Shanghai reflects a more balanced strategy between maximizing total solar capture and achieving temporal synchronization. This divergence underscores that effective design requires a climate-specific, multi-parameter co-optimization approach rather than relying on generic rules.

3.4. Comparison of air conditioning models with constant and variable COP

The preceding analysis were based on an ideal air conditioning (AC) model with a constant COP. To validate the reliability of the optimization results against the realistic air conditioning systems' operational characteristics, a comprehensive sensitivity analysis was conducted. This section compares the constant COP model against variable COP models that incorporate Part-Load Ratio (PLR). Specifically, the standard ASHRAE linear degradation curve was utilized for constant-speed systems, while a quadratic curve was applied for variable-frequency systems.

As shown in Figs. 19 and 20, the comparative sensitivity analysis of dynamic energy matching performance were presented in Guangzhou and Shanghai, respectively. In these figures, the blue solid lines denote

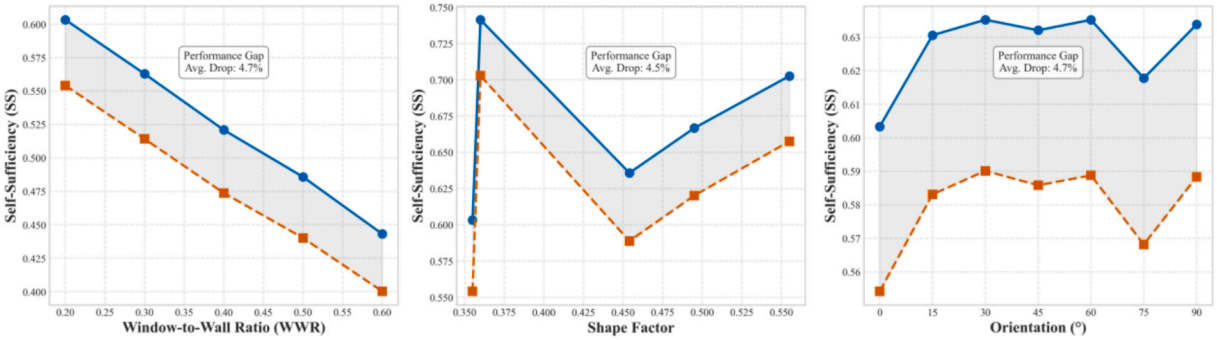


Fig. 19. Comparison of SS value between AC models with constant and variable COP across key parameters in Guangzhou.

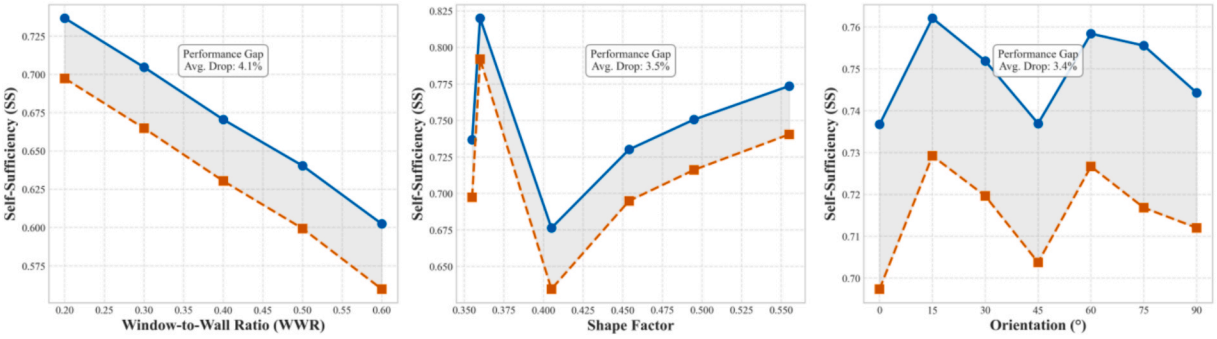


Fig. 20. Comparison of SS value between AC models with constant and variable COP across key parameters in Shanghai.

the results derived from the constant COP model, while the orange dashed lines represent the variable COP model incorporating the linear PLR to simulate realistic operation. As observed, the inclusion of partial load inefficiencies leads to a systematic reduction in SS, with an average drop of 4.1%–4.7% in the corrected model, the characteristic curves remain strictly parallel to the original ideal model. Since both models identically capture the optimization trends for WWR, shape factor, and orientation, the identification of optimal design parameters remains valid regardless of the specific AC modeling approach.

To ensure generalizability across different HVAC technologies, Fig. 21 extends the analysis to a VRF system in Shanghai using a quadratic degradation curve. Under this scenario, the performance gap widens significantly, resulting in an average SS reduction of approximately 15.0%–17.0%, which reflects the severe efficiency penalty imposed during frequent low-load operation. However, even with this substantial absolute deviation, the relative ranking of design parameters remains unaffected. As the inflection points and impact slopes in the VRF model align perfectly with the ideal baseline, this confirms that the optimization trends are preserved regardless of the specific severity of the efficiency degradation curve.

4. Conclusion

With the rapid development of BIPV types, PV direct-driven air conditioning (PVAC) systems emerge as a highly promising solution with significant potential to achieve the goal of real-time zero energy buildings. Building parameter optimization is critical for improving dynamic energy matching degree of PVAC systems, acting on both energy supply and demand. However, a systematic framework that captures the interactive effects of these parameters on dynamic energy matching is still needed to fully realize their potential in PVAC-BIPV systems. In this study, a dynamic energy matching evaluation and optimization of PVAC systems integrated with different BIPV types were introduced in different climatic regions. By incorporating the energy interactions between PV modules and the building envelope, and extending the analysis to the interactive effects of multiple building design parameters, this work provides a more scientific and practical tool for designing nearly zero-energy buildings. The following conclusions are made:

(1) Differing from conventional energy-efficient building design, the impact of building design parameters on the energy matching is fundamentally non-linear.The SS exhibit a “V-shaped” relationship with the Shape Factor, driven by the trade-off between increased heat gain from a larger envelope and the benefit of expanded PV generation area. SS shows a non-monotonic response to Orientation. Different azimuth angles result in distinct diurnal PV generation profiles, process seeks the orientation that best aligns peak generation with peak cooling demand. This highlights that a simplistic strategy of merely minimizing or maximizing individual parameters is insufficient for achieving optimal energy matching.

(2) The univariate effect strength analysis identified a clear hierarchy of influence among design parameters. The Shape Factor consistently exerts the most dominant effect on SS, with a Mean Strength reaching up to 5.38 in Guangzhou, followed by the WWR and then orientation. This hierarchy confirms that geometric parameters governing the magnitude of PV generation and thermal load (Shape Factor and WWR) impose a more primary constraint on energy matching potential than does the temporal alignment of those two factors (Orientation).

(3) Parametric interaction effects proved crucial for system optimization. The synergy between Shape Factor and WWR was the most dominant interaction, with a Mean Strength of 0.0491 in Guangzhou, over 50% higher than in Shanghai. This dominance is rooted in the synergistic and amplifying mechanism between the two parameters, where the shape factor acts as a geometric scaling factor for the thermal and electrical consequences of WWR changes, yielding a total SS improvement of up to 33.58% in Guangzhou.

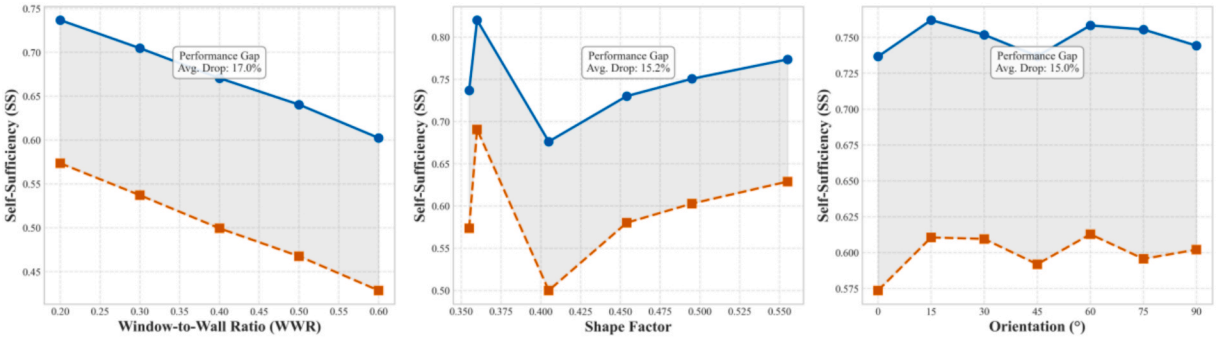


Fig. 21. Comparison of SS value between AC models with constant and variable COP of VRF system in Shanghai.

(4) The holistic, multi-parameter optimization yielded distinct, climate-adaptive design solutions. This integrated optimization achieved peak SS values of 83.84% and 76.26% in Shanghai and Guangzhou, with parameter sets (45°, 0.555, 0.2) and (60°, 0.555, 0.2) respectively, against baselines of 54.25% and 34.32%. This divergence in optimal orientation underscores that effective design necessitates a climate-specific, multi-parameter co-optimization approach over reliance on generic rules.

It is important to acknowledge that the quantitative results presented herein are based on an ideal HVAC model. As verified by the sensitivity analysis, realistic partial-load efficiency degradation systematically reduces the absolute self-sufficiency values by approximately 4% to 5%. However, the optimization trends remain strictly parallel, confirming that the identified optimal design strategies are robust and valid for early-stage decision-making. Furthermore, as the findings are derived from specific case studies in Shanghai and Guangzhou, the direct application of these quantitative benchmarks should be limited to similar subtropical climate zones. Further research is warranted to validate and adapt the framework for other climatic regions, such as arid or continental climates, where the balance between heating and cooling demands would significantly alter the optimization landscape.

CRediT authorship contribution statement

Sihui Li: Writing – original draft, Funding acquisition, Formal analysis, Data curation, Conceptualization. **Li Xie:** Validation, Software, Investigation. **Meng Wang:** Writing – review & editing, Resources, Funding acquisition. **Houpei Li:** Writing – review & editing, Validation, Supervision. **Chujie Lu:** Validation, Software.

Declaration of competing interest

The authors declare that they have no known competing financial interests or personal relationships that could have appeared to influence the work reported in this paper.

Acknowledgement

This work was supported by the National Natural Science Foundation of China (Grant No. 52408100 and No. 52108070), the Natural Science Foundation of Hunan Province (Grant No. 2023JJ40038 and No. 2025JJ50285), the Opening Fund of Key Laboratory of Building Safety and Energy Efficiency of Ministry of Education (Grant No. 2024BSEE00X).

Appendix

Table A1
List of the 25 case combinations for Shape Factor and WWR optimization.

Case No.	Shape Factor (S)	Window-to-Wall Ratio (WWR)
1	0.355	0.2
2	0.355	0.3
3	0.355	0.4
4	0.355	0.5
5	0.355	0.6
6	0.405	0.2
7	0.405	0.3
8	0.405	0.4
9	0.405	0.5
10	0.405	0.6
11	0.454	0.2
12	0.454	0.3
13	0.454	0.4
14	0.454	0.5
15	0.454	0.6
16	0.495	0.2
17	0.495	0.3
18	0.495	0.4
19	0.495	0.5
20	0.495	0.6
21	0.555	0.2
22	0.555	0.3
23	0.555	0.4
24	0.555	0.5
25	0.555	0.6

Data availability

The authors do not have permission to share data.

References

[1] A. Ahmed, T. Ge, J. Peng, et al., Assessment of the renewable energy generation towards net-zero energy buildings: a review, Energ. Buildings 256 (2022) 111755, https://doi.org/10.1016/j.enbuild.2021.111755.
[2] R. Moschetti, H. Brattebø, M. Sparrevik, Exploring the pathway from zero-energy to zero-emission building solutions: a case study of a Norwegian office building, Energ. Buildings 188 (2019) 109666, https://doi.org/10.1016/j.enbuild.2019.01.047.
[3] S. Li, J. Peng, M. Wang, et al., Approaching nearly zero energy of PV direct air conditioners by integrating building design, load flexibility and PCM, Renew. Energy 221 (2024) 119637, https://doi.org/10.1016/j.renene.2023.119637.
[4] R.J. Yang, S.T. Imalka, W.M.P. Wijeratne, et al., Digitalizing building integrated photovoltaic (BIPV) conceptual design: a framework and an example platform, Build. Environ. 243 (2023) 110675, https://doi.org/10.1016/j.buildenv.2023.110675.
[5] M. Wang, X. Zhao, S. Li, et al., Analysis of energy performance and load matching characteristics of various building integrated photovoltaic (BIPV) systems in office building, J. Build. Eng. 96 (2024) 110313, https://doi.org/10.1016/j.jobe.2024.110313.

[6] M. Hummon, P. Denholm, R. Margolis, Impact of photovoltaic orientation on its relative economic value in wholesale energy markets, Prog. Photovolt. Res. Appl. 21 (7) (2013) 1531–1540, https://doi.org/10.1002/pip.2198.
[7] C.M. Hsieh, Y.A. Chen, H. Tan, et al., Potential for installing photovoltaic systems on vertical and horizontal building surfaces in urban areas, Sol. Energy 93 (2013) 150–160, https://doi.org/10.1016/j.solener.2013.04.021.
[8] H.M. Lee, J.H. Yoon, Power performance analysis of a transparent DSSC BIPV window based on 2 year measurement data in a full-scale mock-up, Appl. Energy 225 (2018) 869–879, https://doi.org/10.1016/j.apenergy.2018.04.086.
[9] S. Freitas, C. Reinhart, M.C. Brito, Minimizing storage needs for large scale photovoltaics in the urban environment, Sol. Energy 159 (2018) 375–389, https://doi.org/10.1016/j.solener.2017.11.011.
[10] V. Reis, R.H. Almeida, J.A. Silva, et al., Demand aggregation for photovoltaic self-consumption, Energy Rep. 5 (2019) 981–988, https://doi.org/10.1016/j.egyr.2018.11.002.
[11] S. Li, J. Peng, B. Zou, et al., Zero energy potential of photovoltaic direct-driven air conditioners with considering the load flexibility of air conditioners, Appl. Energy 304 (2021) 117821, https://doi.org/10.1016/j.apenergy.2021.117821.
[12] M. Hartner, A. Ortner, A. Hiesl, et al., East to west – the optimal tilt angle and orientation of photovoltaic panels from an electricity system perspective, Appl. Energy 160 (2015) 94–103, https://doi.org/10.1016/j.apenergy.2015.08.097.
[13] C. Ballif, L.E. Perret-Aebi, S. Lufkin, et al., Integrated thinking for photovoltaics in buildings, Nat. Energy 3 (6) (2018) 438–442, https://doi.org/10.1038/s41560-018-0176-2.
[14] H. Li, J. Li, S. Li, et al., Matching characteristics and AC performance of the photovoltaic-driven air conditioning system, Energy 264 (2023) 126509, https://doi.org/10.1016/j.energy.2022.126509.
[15] M.C. Brito, S. Freitas, S. Guimarães, et al., The importance of facades for the solar PV potential of a Mediterranean city using LiDAR data, Renew. Energy 111 (2017) 85–93, https://doi.org/10.1016/j.renene.2017.03.085.
[16] T.I. Samarasinghalage, W.M.P.U. Wijeratne, R.J. Yang, et al., A multi-objective optimization framework for building-integrated PV envelope design balancing energy and cost, J. Clean. Prod. 342 (2022) 130930, https://doi.org/10.1016/j.jclepro.2022.130930.
[17] S.S. Bhuvad, Udayraj, Investigation of annual performance of a building shaded by rooftop PV panels in different climate zones of India, Renew. Energy 189 (2022) 1361–1379, https://doi.org/10.1016/j.renene.2022.03.004.
[18] D. Wang, T. Qi, Y. Liu, et al., A method for evaluating both shading and power generation effects of rooftop solar PV panels for different climate zones of China, Sol. Energy 205 (2020) 432–445, https://doi.org/10.1016/j.solener.2020.05.009.
[19] E.D. Giouri, M. Tenpierik, M. Turrin, Zero energy potential of a high-rise office building in a Mediterranean climate: using multi-objective optimization to understand the impact of design decisions towards zero-energy high-rise buildings, Energ. Buildings 209 (2019) 109666, https://doi.org/10.1016/j.enbuild.2019.109666.
[20] L.D.Q. Corrêa, D. Bagnis, P.R.M. Franco, et al., Evaluating energy generation of a building-integrated organic photovoltaic vertical façade: a case study of Latin America's pioneering installation, Renew. Energy 220 (2024) 119662, https://doi.org/10.1016/j.renene.2023.119662.
[21] J. Jie, H. Wei, H.N. Lam, The annual analysis of the power output and heat gain of a PV-wall with different integration mode in Hong Kong, Sol. Energy Mater. Sol. Cells 71 (4) (2002) 435–448, https://doi.org/10.1016/S0927-0248(01)00098-8.
[22] G.Y. Yun, M. McEvoy, K. Steemers, Design and overall energy performance of a ventilated photovoltaic façade, Sol. Energy 81 (3) (2007) 383–394, https://doi.org/10.1016/j.solener.2006.06.016.
[23] Y. Wang, W. Tian, J. Ren, et al., Influence of a building's integrated-photovoltaics on heating and cooling loads, Appl. Energy 83 (9) (2006) 989–1003, https://doi.org/10.1016/j.apenergy.2005.10.002.
[24] W.L. Schram, E. Shirazi, PV on façades: a financial, technical and environmental assessment, Energ. Buildings 328 (2025) 115010, https://doi.org/10.1016/j.enbuild.2024.115010.
[25] V.Z. Gjorgievski, N.G. Chatzigeorgiou, V. Venizelou, et al., Evaluation of load matching indicators in residential PV systems-the case of Cyprus, Energies 13 (20) (2020) 5352, https://doi.org/10.3390/en13081934.
[26] L.J. Houchmand, M. Macarulla Martí, S. Gassó-Domingo, Influence of PV panels on convective heat flux in different roofs in the Mediterranean: effects on the urban heat island, Build. Environ. 266 (2024) 112097, https://doi.org/10.1016/j.buildenv.2024.112097.
[27] X. Feng, T. Ma, Y. Yamaguchi, et al., Potential of residential building integrated photovoltaic systems in different regions of China, Energy Sustain. Dev. 72 (2023) 1–13, https://doi.org/10.1016/j.esd.2022.11.006.
[28] C. Koo, T. Hong, K. Jeong, et al., Development of the smart photovoltaic system blind and its impact on net-zero energy solar buildings using technical-economic-political analyses, Energy 124 (2017) 382–396, https://doi.org/10.1016/j.energy.2017.02.088.
[29] D. Aelenei, R.A. Lopes, L. Aelenei, et al., Investigating the potential for energy flexibility in an office building with a vertical BIPV and a PV roof system, Renew. Energy 137 (2019) 189–197, https://doi.org/10.1016/j.renene.2018.07.140.
[30] H. Zhou, H. Yang, J. Peng, Solar PV vacuum glazing (SVG) insulated building facades: thermal and electrical performances, Appl. Energy 376 (2024) 124323, https://doi.org/10.1016/j.apenergy.2024.124323.
[31] C. Liu, W. Xu, A. Li, et al., Analysis and optimization of load matching in photovoltaic systems for zero energy buildings in different climate zones of China, J. Clean. Prod. 238 (2019) 117914, https://doi.org/10.1016/j.jclepro.2019.117914.
[32] R. Wattan, S. Janjai, An investigation of the performance of 14 models for estimating hourly diffuse irradiation on inclined surfaces at tropical sites, Renew. Energy 93 (2016) 667–674, https://doi.org/10.1016/j.renene.2016.02.076.
[33] A.K. Shukla, K. Sudhakar, P. Baredar, Design, simulation and economic analysis of standalone roof top solar PV system in India, Sol. Energy 136 (2016) 437–449, https://doi.org/10.1016/j.solener.2016.07.009.
[34] M. Zandi, M. Bahrami, S. Eslami, et al., Evaluation and comparison of economic policies to increase distributed generation capacity in the Iranian household consumption sector using photovoltaic systems and RETScreen software, Renew. Energy 107 (2017) 215–225, https://doi.org/10.1016/j.renene.2017.01.051.
[35] S. Yilmaz, H.R. Ozcalik, M. Aksu, et al., Dynamic simulation of a PV-diesel-battery hybrid plant for off grid electricity supply, Energy Procedia 75 (2015) 396–402, https://doi.org/10.1016/j.egypro.2015.07.396.
[36] H. Hossei, K.H. Kim, Assessing the PV-integrated south facade in mitigating the BIPV system oversupply, Energy Rep. 12 (2024) 4594–4606, https://doi.org/10.1016/j.egyr.2024.10.023.
[37] C. Vassiliades, Optimizing energy efficiency in mediterranean single-family homes: a parametric study of building typology, orientation, and BIPV integration, Renew. Energy 237 (2024) 121541, https://doi.org/10.1016/j.renene.2024.121541.
[38] A. Chatzipanagi, F. Frontini, A. Virtuani, BIPV-temp: a demonstrative Building Integrated Photovoltaic installation, Appl. Energy 173 (2016) 1–12, https://doi.org/10.1016/j.apenergy.2016.03.097.
[39] R. Gottschalg, T.R. Betts, S.R. Williams, et al., A critical appraisal of the factors affecting energy production from amorphous silicon photovoltaic arrays in a maritime climate, Sol. Energy 77 (6) (2004) 909–916, https://doi.org/10.1016/j.solener.2004.06.015.
[40] A.M.A. Youssef, Z.J. Zhai, R.M. Reffat, Genetic algorithm based optimization for photovoltaics integrated building envelope, Energ. Buildings 127 (2016) 1093–1102, https://doi.org/10.1016/j.enbuild.2016.06.018.
[41] A. Azami, H. Sevinç, The energy performance of building integrated photovoltaics (BIPV) by determination of optimal building envelope, Build. Environ. 199 (2021) 107856, https://doi.org/10.1016/j.buildenv.2021.107856.
[42] G.K. Oral, Z. Yilmaz, Building form for cold climatic zones related to building envelope from heating energy conservation point of view, Energ. Buildings 35 (4) (2003) 383–388, https://doi.org/10.1016/S0378-7788(02)00111-1.
[43] C. Zomer, I. Custódio, A. Antoniolli, et al., Performance assessment of partially shaded building-integrated photovoltaic (BIPV) systems in a positive-energy solar energy laboratory building: Architecture perspectives, Sol. Energy 211 (2020) 869–880, https://doi.org/10.1016/j.solener.2020.10.026.
[44] A.K. Shukla, K. Sudhakar, P. Baredar, A comprehensive review on design of building integrated photovoltaic system, Energ. Buildings 128 (2016) 99–110, https://doi.org/10.1016/j.enbuild.2016.06.077.
[45] F. Gao, J.B. Chen, L. Weng, Experimental study on heat dissipation performance of photovoltaic walls with air flow passages, Building Energy Efficiency 47 (4) (2019) 50–53.
[46] J. Hyun, B. Park, N. Kim, et al., Building energy performance of DSSC BIPV windows in accordance with the lighting control methods and climate zones, Sol. Energy 244 (2022) 279–288, https://doi.org/10.1016/j.solener.2022.08.046.
[47] M. Chung, B. Park, E. Choi, et al., Performance level criteria for semi-transparent photovoltaic windows based on dye-sensitized solar cells, Sol. Energy Mater. Sol. Cells 217 (2020) 110683, https://doi.org/10.1016/j.solmat.2020.110683.